AN ALTERNATIVE PROCEDURE TO MEASURE RAILROAD TRACK IRREGULARITIES. APPLICATION TO A SCALED TRACK

Javier F. Aceituno[1,*], Rosario Chamorro[2], Sergio Muñoz[3], José L. Escalona[2]

[1]*Departamento de Ingeniería Mecánica y Minera. Universidad de Jaén (Spain)*

[2]*Departamento de Ingeniería Mecánica y de Fabricación. Universidad de Sevilla (Spain)*

[3]*Departmento de Ingeniería y Ciencia de los Materiales y del Transporte. Universidad de Sevilla (Spain)*

Abstract

In this paper an alternative procedure to accurately measure static railroad track irregularities is proposed and applied to a scaled railroad track. The purpose of this work is the determination of highly-precise measured data in short track segments that needs to be used as input in the validation of railroad computational models that are used for on-board railroad track measurement systems. The procedure consists of the use of a topographic total station combined with a postprocessing of the measured data that reduces misalignment errors and provide the analytical ideal geometry of the track together with its irregular geometry characterized in terms of the magnitudes of track gauge, vertical profile, alignment and cross level. Experimental results are compared to standard magnitudes of full scale tracks showing that real track geometry can differ from PSD-based predicted one. This supports the application of the proposed procedure for an accurate geometric determination of short track segments.

Keywords: *Railroad track measurement; Track irregularities; Ideal track geometry; Error minimization*

[*]Corresponding author. *Tel.*: +34 953648619. *E-mail address:* jaceitun@ujaen.es (Javier F. Aceituno)
Address: Campus Científico-Tecnológico, Cinturón Sur, 23700, Linares, Jaén, (Spain)

1. INTRODUCTION

When analyzing the dynamics of railroad vehicles, it is fundamental to accurately account for the vehicle/track interaction to obtain realistic results that lead to objective conclusions. In this sense, the influence that track irregularities have in the wheel/rail contact scenario and consequently, in the dynamic behavior of the vehicle, is of major importance [1]. They can be considered as lateral and vertical deviations of the rails cross-sections with respect to a reference configuration, usually referred as the mean line position of the perfect track or track centerline.

In the literature, track irregularities are traditionally modeled as random stochastic processes and characterized by the use of a one-sided power spectral density (PSD) functions of the track geometry [2, 3]. Its geometry characterization and categorization can be given by different regulations such as the European standard EN-13848 series [4] or by the Federal Railroad Administration (FRA) in their track safety standards [5, 6], where six categories represent the different qualities of the tracks being Class 6 the best-quality track and Class 1 the worst-quality one. This random stochastic characterization of track geometry has derived in many research publications for the analysis of alternative methods to generate accurate and representative track irregularities. Fries and Coffey [7] presented a method to generate random vertical and cross level irregularities as inputs to numerical simulations showing a good agreement for the spectral characteristic of a measured Class 4 track. Claus and Schiehlen [3] discussed and compared the representation of track irregularities by PSD functions with experimental measurement data derived by the German Railways Deutsche Bahn AG. Also, Perrin et al. [8] developed a stochastic modeling of the track geometry and its identification with experimental measurements. In this work, the statistical properties of the non-Gaussian and non-stationary track irregularity random field [9] are identified based on the experimental database provided by the measurement train IRIS 320 running over the French railway network.

Regarding the measurement of the track quality there are different techniques available whose applicability depends on the measuring systems and instrumentation used. As presented in Stow and Andersson [10], these measuring techniques can be classified in three types: (1) manual survey, (2) track geometry trolley and (3) track recording vehicles.

Manual survey allows left and right rail positions measurement with reference to a fixed ground position. Although they provide accurate results, they are slow to carry out and therefore limited to short sections of the track. An interesting technique is presented by Yao et al. [11] where an approach that uses a laser tracker to detect static track irregularities using a reflecting target on the top of a trolley is proposed. This approach is compared to a track geometry trolley showing relatively good agreement with faster results. However, differences in measurements are attributed to the influence of the dynamics of the trolley that carries the target prism. In Psimoulis and Stiros [12], a specific application of a manual survey using a robotic total station to measure the deflections of a short-span bridge in response to passing trains is presented. Although in a previous work they concluded that the accuracy of measurements lowered for targets moving with velocities higher than 15 cm/s [13], this inconvenience is no longer present as modern total stations develop higher sampling rates of measurements [12].

The use of track geometry trolleys is another commonly used technique where instrumentation is installed on a trolley. These systems, which are usually manually-pushed, are limited by the capability of the on-board data logger, power supplies and speed of recording, that can be in a stop-and-go mode or continuous mode. However, this limited speed of operation can be an

advantage for those that conduct continuous measurements as the influence that the dynamics of the trolley has on measurements is minimum. Special attention should be focus to the work of Chen et al. [14], where a modular track geometry measuring trolley is design based on an aided inertial navigation system to be used for different surveying tasks such as the measurement of track irregularities, tamping or adjustment of slab track. The proposed trolley system gives track measurements whose accuracy conforms to the requirement of the normative standards but increases the surveying efficiency by orders of magnitude. In addition to this modular trolley, a classical measuring one can be found in the work of Akpinar et al. [15] where a multisensory railway track geometry surveying system based on Global Navigation Satellite System (GNSS), linear variable differential transformers (LVDT), inclinometers and a total station is designed to control railroad track geometry. In this trolley, the adaptive Kalman filtering algorithm used for determining the track geometry is described in [16].

Concerning track recording vehicles (TRV), they are equipped with an acquisition system formed by accelerometers, LVDTs, lasers and cameras that measure the track geometry as they run over the track. Their highest inconvenience is that the dynamics of these vehicles clearly influences the measurements and therefore an offline postprocess of the information given by sensors is required. Nevertheless, due to the advantages that the speed of operation of these TRV vehicles have, much research work has been done in this field especially with the idea of transform most railroad vehicles into TRV ones. In this context the work of Weston et al. [17] presents the state of the art in the monitoring of track geometry condition from in-service vehicles. The main conclusion of this work is that, besides the inaccuracies produced by the dynamic behavior of vehicles, observing track geometry quality and its degradation repeatedly and transmitting this information to a central server has become a reality within the past decade. In this research line, the following works are highlighted [18-22]. In [18, 19], the monitoring of the vertical and lateral irregularity from in-service railroad vehicles is presented. While the accuracy in the estimation of vertical irregularities is excellent, the estimation of lateral ones presents higher inaccuracies due to vehicles lateral motion. In [20], a system that also identifies vertical and lateral track geometry irregularities using accelerometers placed on the body of Japanese in-service vehicles is described and validated against measurements of a dedicated TRV vehicle. Also, as shown more recently by Karis et al. [21], a comparison between the measurements of two ATC vehicles (DynoTrain and Swedish Green Train) with the dynamic response of three vehicles is derived and proved that axlebox accelerations and track irregularities present the highest correlation. Additionally, it is also interesting the work of Taheri Andani et al. [22] where a non-contact track monitoring instrument based on doppler light detection technology on-board railroad vehicles for determining precisely lateral irregularities is investigated.

The differences among these three different measuring techniques imply that it exists no available one capable of determining rail track geometry in their whole wavelength range through considerable distances, currently due to technical difficulties. This conclusion is confirmed in the work of Nielsen et al. [23] where a detailed analysis of the rail track measuring systems to detect irregularities employed in European countries is derived. They conclude that European standard EN-13848 [4] should be modified to account for those short-wavelength irregularities which are not considered.

The procedure presented in this work can be categorized as a manual survey technique that seeks an accurate determination of static track defects by the use of a total station and a manually-pushed reflecting target located at the top of the rail heads. The applicability of this methodology, regardless of the short track segments that can be measured, is in the validation of computational

railroad simulation models that can used in the on-board estimation of track irregularities with in-service vehicles or in the estimation of other critical parameters of the rolling stock, such as vehicle critical speed [24] or vibration attenuation [25]. For these applications the accuracy of the track geometry is of major importance. As an example, we applied the proposed method for the geometric evaluation of a scaled track that is used in the validation of computational models and compared the measured geometry with that estimated using analytical PSD-functions found in the literature. Results show that this approach gives an adequate and simple solution for tracks were experimental tests are carried out.

The paper is organized as follows: in Section 2, a brief description of the definition of the railroad track geometry is presented. Section 3 details the proposed procedure to accurately measure the railroad track geometry and the postprocessing methodology to minimize errors. Section 4 presents the computation of the track irregularities based on the postprocessed measured data and on the ideal track configuration. In Section 5, this procedure is applied to measure the geometry of a scaled 5-inch gauge railroad track giving results that are properly scaled and compared to the geometry of a full-scale track. Finally, Section 6 provides some conclusions and a summary.

2. RAILROAD TRACK GEOMETRY

The real geometry of a railroad track is obtained as a superposition of its ideal or theoretical geometry and its irregularities. In this section, a brief description of these definitions is presented.

2.1 IDEAL RAILROAD TRACK DEFINITION

The definition of the ideal geometry is formed by the horizontal and vertical profiles, which can be given by several stretches. The railroad track horizontal description is made up of three different stretches: straights (tangents), circumferences (curves) and transitions (clothoids) while for the vertical description, straight and transitions stretches are usually defined [26]. These track segments, which are joined by vertices, do not necessarily have to coincide between the horizontal and vertical characterizations.

The parameters used to characterize the geometry of each track segment are:

- Horizontal curvature, ρ_h
- Vertical curvature, ρ_v
- Twist curvature, ρ_{tw}
- Derivative of the horizontal curvature, ρ'_h
- Vertical slope, α_v

And the values of these parameters for each kind of stretch are given in Table 1, where R_h is the curve radius, $f_{lin}(s)$ is a lineal function of the trajectory coordinate s (see Fig. 1) in the range of 0 and 1 value, being 0 at the vertex in the straight stretch and 1 at the vertex in the curve one. φ_p is the superelevation angle, L_{ht} and L_{vt} are the horizontal and vertical stretches length respectively and α_{v1} and α_{v2} are vertical slopes of the straight segments before and after the transition.

Table 1. Track geometry parameters in the horizontal and vertical characterization.

Horizontal description			
Straight	$\rho_h = 0$	$\rho_{tw} = 0$	$\rho'_h = 0$
Curve	$\rho_h = 1/R_h$	$\rho_{tw} = \varphi_p$	$\rho'_h = 0$
Transition	$\rho_h = f_{lin}(s)\cdot 1/R_h$	$\rho_{tw} = f_{lin}(s)\varphi_p$	$\rho'_h = 1/(L_{ht}\cdot R_h)$
Vertical description			
Straight	$\alpha_v = constant$		
Transition	$\alpha_v = \alpha_{v1} + f_{lin}(s)\cdot(\alpha_{v2} - \alpha_{v1})$		$\rho_v = (\alpha_{v2} - \alpha_{v1})/L_{vt}$

As usually done in the railroad industry for the design of the ideal geometry of the railroad track, the position vector of an arbitrary point of the track centerline, $\mathbf{r}^t$, is obtained by the analytical expressions of Table 1. This way, the heading angle ψ^t , the vertical slope of the track centerline θ^t and the superelevation angle φ^t, which are shown in Fig. 1, can be defined as:

$$\begin{aligned} \psi^t(s) &= \operatorname{atan}2\left(\frac{dr_y^t/ds}{dr_x^t/ds}\right) \\ \theta^t(s) &= \operatorname{atan}\left(\frac{dr_z^t}{ds}\right) \\ \varphi^t(s) &= \rho_{tw}(s) \end{aligned} \tag{1}$$

where r_x^t, r_y^t and r_z^t are the Cartesian components of vector $\mathbf{r}^t$.

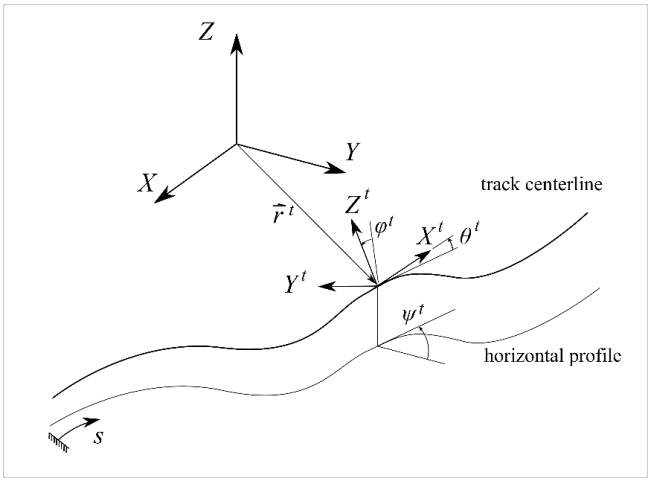

Figure 1. Description of track centerline geometry

2.2 TRACK IRREGULARITIES

Railroad track irregularities can be considered as geometrical deviations of the railheads from their ideal positions (see Fig. 2). There are two categories to characterize them: isolated and distributed track defects [6].

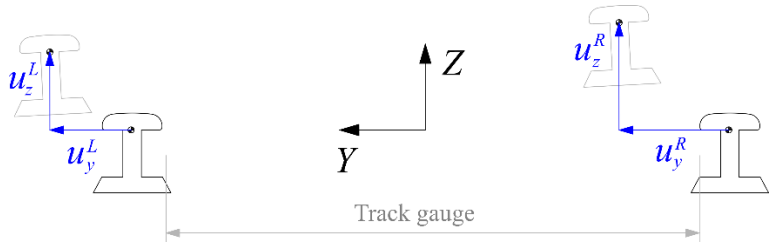

Figure 2. Rail heads deviations from the ideal position

Isolated track defects, which are the main cause of unsafe responses, are exceptional cases that appear rarely. They are usually present at special track work, in poor drainage areas, and at road crossings, bridges or turnouts. Their frequency of happening depends on the track features, but their relevant influence on vehicle dynamics requires a special care when dealing with them.

Distributed track irregularities are present along the railroad track having regular patterns. In the railway industry, they are defined as track centerline irregularities in the following four well-known measurements shown in Fig. 3: track gauge variation ζ_g, lateral alignment ζ_a, cross level ζ_{cl}, and vertical profile ζ_{vp} [5]. They can be defined as:

$$\begin{aligned} \zeta_g &= \left(u_y^L - u_y^R\right), \quad \zeta_a = \left(u_y^L + u_y^R\right)/2 \\ \zeta_{cl} &= \left(u_z^L - u_z^R\right), \quad \zeta_{vp} = \left(u_z^L + u_z^R\right)/2 \end{aligned} \tag{2}$$

where as it is shown in Fig. 2, u_y^L, u_y^R, u_z^L and u_z^R are the lateral and vertical left and right railheads deviation respectively.

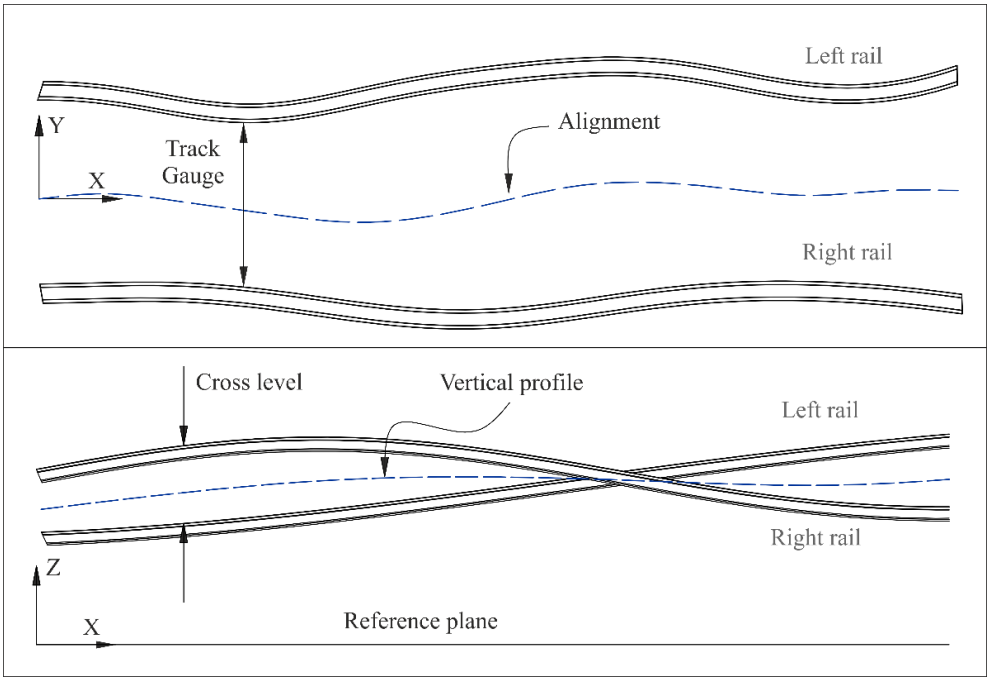

Figure 3. Track irregularity measurements

3. TRACK MEASUREMENT PROCEDURE

As it is mentioned in the introduction of this work, the current techniques applied for the measurement of the track geometry employ the use of automatic track recording vehicles or the use of manual trolleys that accurately measure track geometry as they roll over the track. However, as this work faces the necessity of accurately measure a scaled railroad track with the final purpose of validating computational models, these techniques cannot directly be applied mainly due to two reasons; the size difference between the real and scaled track, and the direct influence of the recording-vehicle dynamics in the measurements.

To avoid these inconveniences, an alternative procedure based on the use of a topographic total station to conduct measurements *in repose* is presented. The main advantage of this procedure is the capability to obtain highly-precise and direct measured data with a low-cost investment, which is in accordance to the purpose of this work. In addition, as there is no need to account for a large track geometry, which would be disadvantageous in this method for time reasons, the use of this technique results the most appropriate one.

Therefore, the general procedure to account for the track geometry using a topographic total station consists of:

- Positioning of the total station
- Railheads marking
- Track measuring
- Postprocessing of measured data
- Identification of the ideal track centerline geometry
- Computation of track irregularities

In what follows, these seven tasks shown in Fig. 4 are described and then applied to a scaled railroad track that has a nominal track gauge of 5 in. and that is available for this measurement. However, as it will be shown in the next sections, they can be easily adapted to full-scale tracks without any particular modifications.

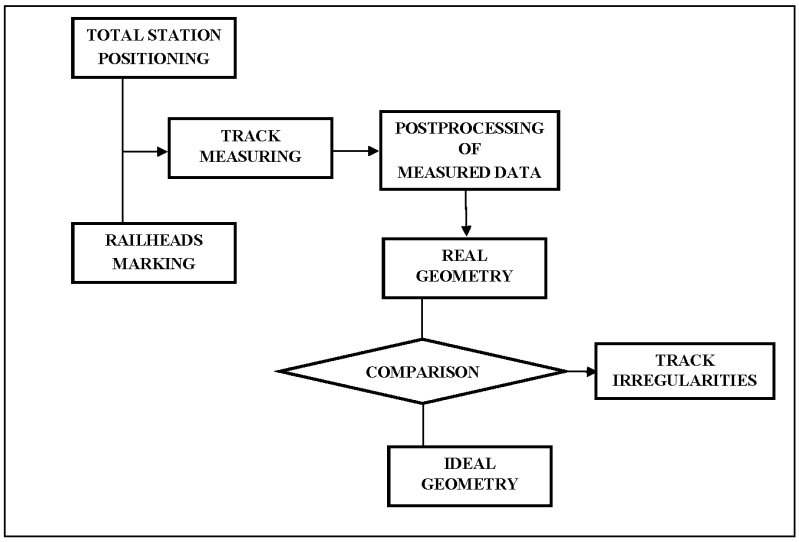

Figure 4. Procedure to measure track irregularities

3.1 POSITIONING, RAILHEADS MARKING AND MEASURING

These three tasks compose the experimental part of the procedure and consist of the appropriate choice of the total station positions, the railheads marking where to conduct the measurements, and the measurement itself.

Regarding the positioning of the total station device, it is of major importance to identify the minimum and most appropriate positions along the track to avoid the presence of obstacles in the direct measurement of the railheads and to minimize errors. Also, the railheads marking sets the points over the railheads that will be measure by the total station. This marking should always be done in the same relative position of the rails, such as the top of the railheads. The distance between consecutive points depends on the irregularity wavelengths that are desired to measure. Some regulations, such as the European prEN 13848-5 [4], classifies three different limits of track irregularities according to their severity. Limit D1 between 3 and 25 m wavelength, D2 between 25 and 70 m. and D3 between 70 and 200 m. Finally, when both rails are marked the track geometry measurement can be done by using a total station device pointing to the marked points.

3.2 POSTPROCESSING OF MEASURED TRACK DATA

When applying this technique, measured points in the left and right rails need to be transformed into quantitative irregularities, such as vertical and lateral displacements of railheads with respect to the undeformed track configuration. This postprocessing of the measured data is particular for each measurement and will require different tasks depending on the process (i.e. measurement organization, changes in the total station position or removal of duplicated points).

However, all measurements have in common that they will require a minimization of the error produced when the total station is changed in position, even after leveling [27]. When the measuring device is changed in position (i.e. when measurements are done in different days or when obstacles require different positions), there is a certain error when orientating it with respect to the original position. This fact can be seen in Fig. 5, where one can see the possible deviation between two different groups of points measured in the same rail. In this figure, the groups of points *A* and *B* are measured before and after the change of the total station position respectively. To quantify this misalignment, a total of 5 points are measured twice, being the vector $\Delta\mathbf{r}^i = \mathbf{r}_A^i - \mathbf{r}_B^i$, the misalignment deviation at point *i*.

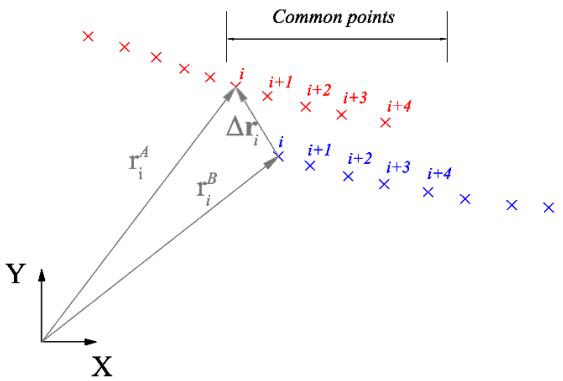

Figure 5. Misalignment estimation in one rail
x: *A* – measured points x: *B* – measured points

In order to minimize this misalignment, the following simple but effective procedure that consists on a constant translation of all points in the *B* group and a rotation of all of them as a rigid body with respect to a selected point is proposed:

- If *A* and *B* are the groups of points measured before and after the change in the total station position respectively:
  - The distance vector $\Delta\mathbf{r}_i$ is computed for each overlapping point *i* at both rails. The minimum $\Delta\mathbf{r}_i$ is selected and its point *i* identified. The global position vector of this point in the *B*-group is called $\overline{\mathbf{r}}^B$.
- As every point in group *B* will be translated a constant vector $\overline{\mathbf{r}}$ and rotated as a rigid body with respect to point *i* a constant angle α in the XY plane, the relative position vectors $\Delta\mathbf{r}_i^B$ of every point in *B* with respect to the selected point, ($\Delta\mathbf{r}_i^B = \overline{\mathbf{r}}^B - \mathbf{r}_i^B$), is computed (see Fig. 6).

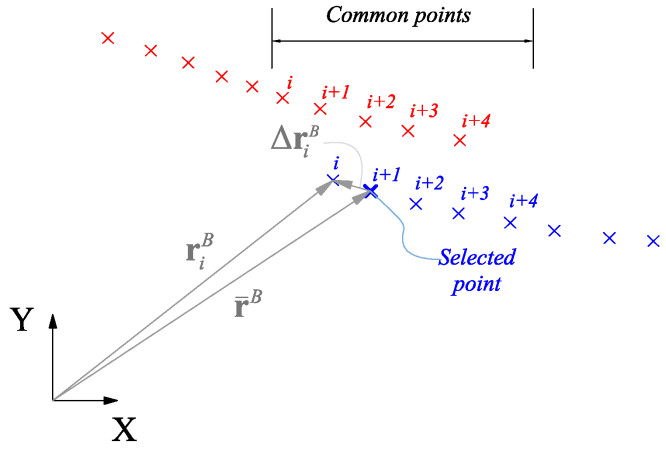

Figure 6. Selected point and relative positions $\Delta\mathbf{r}_i^B$

x: *A* – measured points x: *B* – measured points

- The translation and rotation applied to the *B* points is done by the following expression:

$$\mathbf{r}_i'^B = \overline{\mathbf{r}}^B + \overline{\mathbf{r}} + \mathbf{A}_B\left(\overline{\mathbf{r}}^B - \mathbf{r}_i^B\right) = \overline{\mathbf{r}}^B + \overline{\mathbf{r}} + \mathbf{A}^B\Delta\mathbf{r}_i^B \tag{3}$$

where $\mathbf{r}_i'^B$ is the updated global position vector of a point *i* in the *B* group of points after translation and rotation and $\mathbf{A}^B$ is the transformation matrix that accounts for the rotation angle α as follows:

$$\mathbf{A}^B = \begin{bmatrix} \cos\alpha & -\sin\alpha & 0 \\ \sin\alpha & \cos\alpha & 0 \\ 0 & 0 & 1 \end{bmatrix} \tag{4}$$

Figure 7 shows the final positions of measured points when this process is applied.

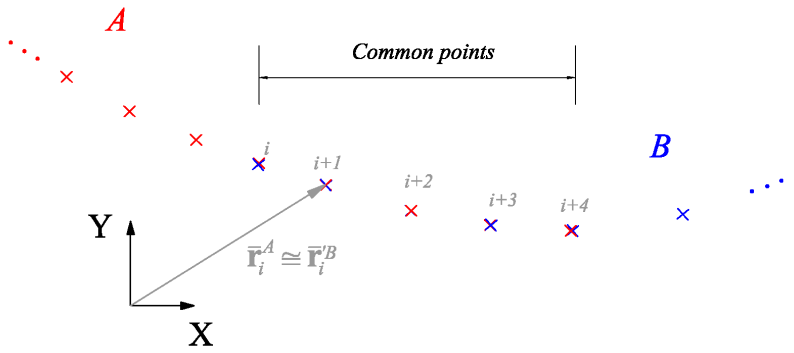

Figure 7. Postprocessed measured points

- In order to compute the translation vector $\overline{\mathbf{r}} = [x, y, z]^T$ and the rotation angle α, a minimization of the function *f,* that is the sum of all quadratic distances d^{i2} between the overlapping points in *A* and translated in *B*, must be done. The quadratic distance d^{i2} for each measured point *i* is defined as:

$$d^{i2} = \left[\mathbf{r}_i^A - \mathbf{r}'^B_i\right]^T \left[\mathbf{r}_i^A - \mathbf{r}'^B_i\right] \tag{5}$$

And the function *f* to minimize

$$f = f(\mathbf{u}) = \sum_{i=1}^{n_c} d^{i2} \tag{6}$$

where n_c is the number of common points and $\mathbf{u}$ is the vector of unknowns whose components are $\mathbf{u} = [x,y,z,\alpha]^T$.

It should be noted that this track alignment adjustment also restores to the correct place the track centerline, which is fundamental for the calculation of track irregularities as shown in the following section.

4. CALCULATION OF TRACK IRREGULARITIES

Once the measured points at the left and right rails are postprocessed, the computation of the track geometry quality can be done. The straightforward procedure consists on quantifying the deviation of the left and right rails with respect to its ideal configuration. However, although the ideal configuration of the track can be known by its construction drawings, it should not be considered as a known geometry, since it is usually common to find great differences between construction drawings and what definitely is built. The objective of calculating the ideal geometry of the track centerline is also explained by the use of railroad simulation packages, which are characterized by the definition of the tracks using the three concepts defined in Section 2 [25, 26]; projection (tangent, curve and transition stretches), development and super-elevation. This work assumes that the ideal geometry of the track centerline is known. However, as this methodology is applied to a scaled railroad track in Section 5 whose ideal geometry is not known, a particular procedure to obtain it is applied. Therefore, assuming a known track centerline, the irregularities

can be quantified by computing the distance difference of the measured points with respect to the ideal position of the right and left rails as shown in Fig. 2.

In case of lateral irregularities, the ideal track gauge has to be centrally translated and superposed along the track centerline as shown in Fig. 8, where for simplicity, only the left rail is considered. This process is described as follows:

- First, the unitary vector for the left rail at point i, $\mathbf{j}^i_L$ can be computed as

$$\mathbf{J}^i_L = \mathbf{r}^i_L - \mathbf{r}^i_{CL} \quad \rightarrow \quad \mathbf{j}^i_L = \frac{\mathbf{J}^i_L}{\left|\mathbf{J}^i_L\right|} \tag{7}$$

  where $\mathbf{J}^i_L$ refers to the position vector between the point i in the left rail and the corresponding point i in the track centerline.
- Then, the track centerline is centrally translated the half-gauge (see Fig. 8). If a is the track half gauge, this translation is obtained as $a\mathbf{j}^i_L$. Consequently, the vector $\mathbf{y}^i_L$ that accounts for the lateral irregularity in the left rail can be calculated as:

$$\mathbf{y}^i_L = \mathbf{r}^i_L - \left(\mathbf{r}^i_{CL} + a\mathbf{j}^i_L\right) \tag{8}$$

- Finally, the lateral left track irregularity at point i, u_y^{Li}, is obtained as the norm of $\mathbf{y}^i_L$ but taking into account its sign to be in accordance with the local frames of Fig. 2. This is, for the left rail, if $\mathbf{r}^i_L$ is larger than $\mathbf{r}^i_{CL} + a\mathbf{j}^i_L$, then u_y^{Li} is positive while for the right rail, if $\mathbf{r}^i_R$ is larger than $\mathbf{r}^i_{CL} + a\mathbf{j}^i_R$, the lateral right irregularity u_y^{Ri} is negative.

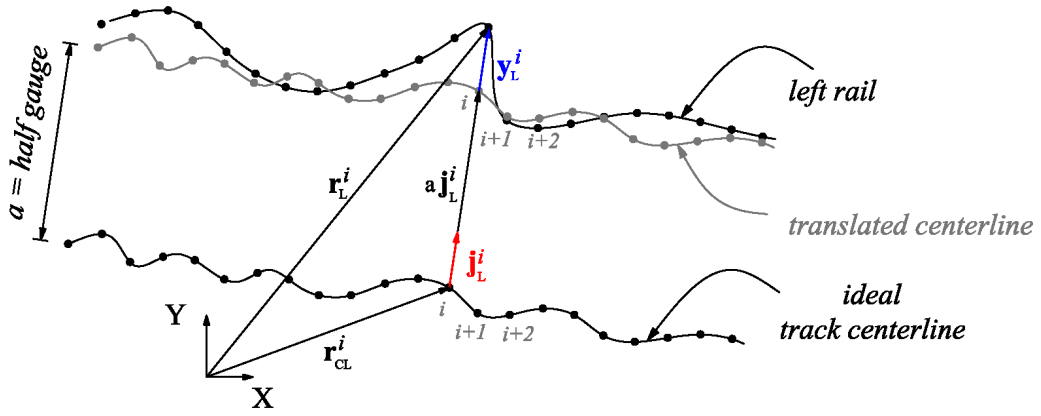

Figure 8. Computation of lateral irregularities in the left rail

Regarding vertical irregularities, a similar procedure can be applied by doing a translation of the vertical component of the ideal track centerline as a function of the cant angle. This allows a clear computation of these irregularities in Eq. 9 as the difference between the vertical component of the ideal left and right railheads, $\mathbf{r}^{ideal}_L$ and $\mathbf{r}^{ideal}_R$, and the vertical component of the left and right measured railheads $\mathbf{r}_L$ and $\mathbf{r}_R$ respectively.

$$\begin{aligned} u^L_z &= \left(\mathbf{r}_L - \mathbf{r}^{ideal}_L\right)_z \\ u^R_z &= \left(\mathbf{r}_R - \mathbf{r}^{ideal}_R\right)_z \end{aligned} \tag{9}$$

After this process is applied to the measured points, lateral and vertical irregularities can be now quantified in terms of the well-known track characteristics of track gauge ζ_g, lateral alignment ζ_a, cross level ζ_{cl}, and vertical profile ζ_{vp} of Eq. 2.

5. APPLICATION TO A SCALED RAILROAD TRACK

In what follows, this track irregularity measurement procedure is applied to a scaled railroad track. First, railheads marking and measuring procedure are briefly presented followed by the postprocessing applied to minimize errors. Then, prior to the computation of track irregularities, the ideal geometry of the scaled track is determined. To finish, the identification of the lateral and vertical railheads deviations is computed and compared to statistical irregular geometry found at full-scale tracks.

5.1 POSITIONING, SCALED RAILHEADS MARKING AND MEASURING

The scaled track is located in city of Sevilla, has a nominal gauge of 5 in. and a length of 68 meters, which is formed by a theoretically 35 m. tangent stretch followed by a 15 m. radius curved one. Due to the track size and assuming that the scaled track experiences irregularities in a different pattern than full scale tracks, a minimum wavelength up to 4 cm. is considered, which implies a manually railhead marking every 2 cm. as shown in Fig. 9 giving a total of 6800 points of measure.

Figure 9. Track railhead marking

Once both rails are marked, the measurement is done using the high-precise Leica Geosystems total station model *TS15 P1" R400*. To help the measurements, a target prism is vertically aligned and positioned in the marked points as shown in Fig. 10.

Figure 10. Track measuring procedure

Figure 11 shows the experimental track measured points classified in 7 different group of points (*A, B, C, D, F, G,* and *H*), which means that the total station was installed in the field seven times in two different positions.

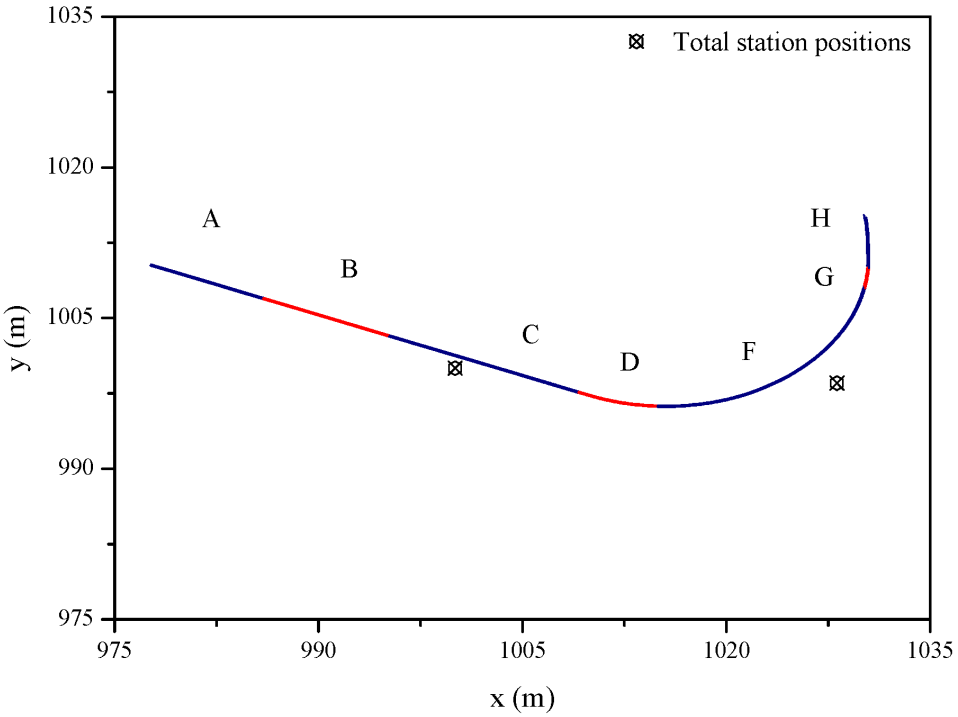

Figure 11. Experimental track measured points

5.2 POSTPROCESSING OF MEASURED TRACK DATA AND ERROR MINIMIZATION

The error produced when orientating the total station with respect to its original position can be seen in Fig. 12, which is a zoom of Fig. 11.

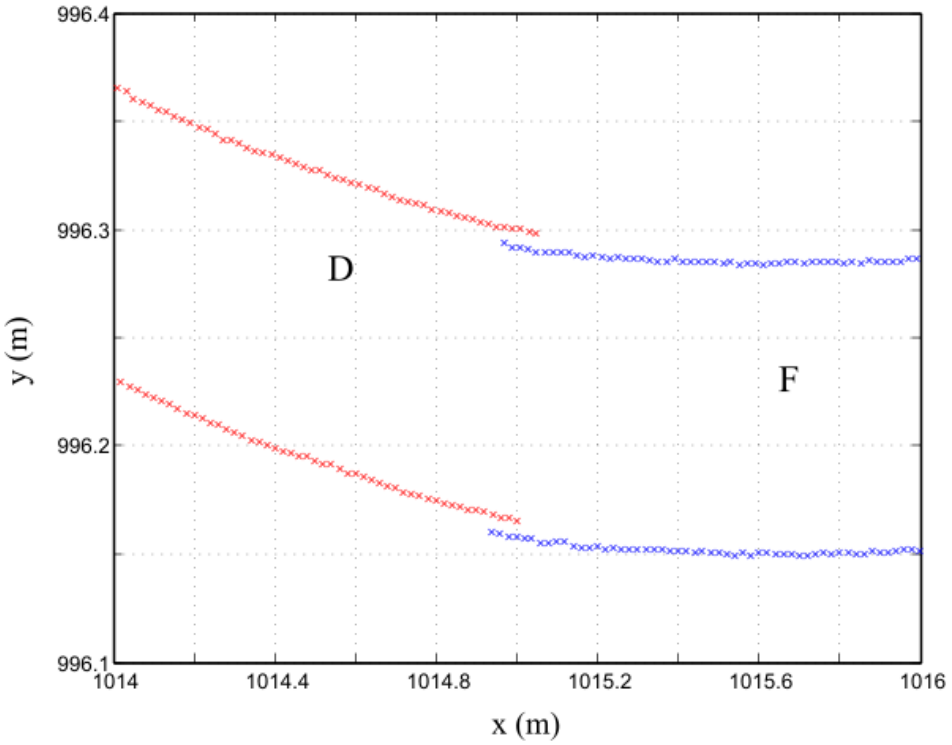

Figure 12. Misalignment error between the *D* and *F* groups of points

As there are 7 different group of points, the translation and rotation procedure presented in Section 3.2.1 is applied stepwise, where each group of points is considered as a single rigid body whose translation and rotation minimizes the quadratic distance d'^2 given in Eqs. (5) and (6). Translation vectors and rotation angles are shown in Table 2:

Table 2. Translation vector and rotation angle in measured group of points

Pair of group of points	$\overline{\mathbf{r}}$ (mm)	α (rad)
H - G	$[-11.58 \quad 3.83 \quad -0.23]^T$	0.0020
HG - F	$[-0.22 \quad 0.20 \quad 0.77]^T$	0.0014
HGF - D	$[\ 0.12 \quad 8.16 \quad -0.08]^T$	-0.0035
HGFD - C	$[-0.29 \quad -0.18 \quad 0.41]^T$	0.0015
HGFDC - B	$[\ -0.16 \quad -0.29 \quad 0.45]^T$	-0.0030
HGFDCB - A	$[-1.96 \quad -2.93 \quad 0.73]^T$	0.0025

Finally, Fig. 13 shows the result obtained after the application of this simple minimization procedure to the whole measured points presented in Fig. 11. It can be seen how the misalignment error between the *D* (red) and *F* (blue) group of points is corrected and transformed into the postprocessed black circled points.

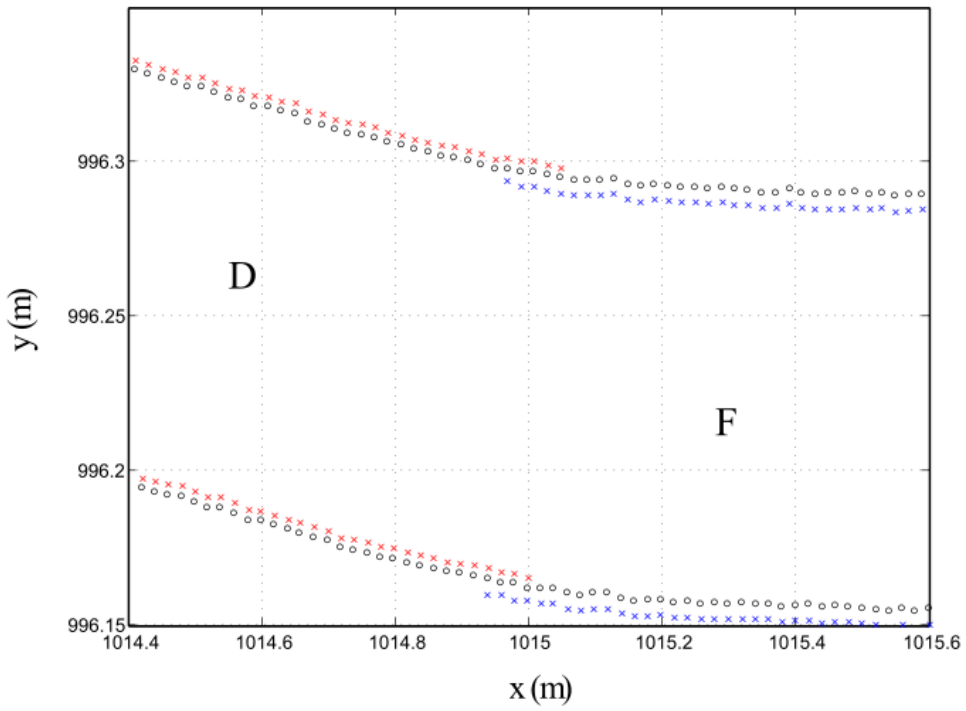

Figure 13. Measured and processed *D* and *F* group of points
x: *D* – measured points x: *F* – measured points o: processed points

5.3 CALCULATION OF THE SCALED TRACK IDEAL GEOMETRY

The computation of the railheads deviations with respect to the ideal geometry requires the knowledge of the ideal one in terms of projection, development and superelevation.

Projection:

To identify the ideal projection of the track centerline, one can refer to the construction drawings to have an initial approximation. In this context, the measured track is theoretically formed by a 35 m. tangent stretch and 15 m. constant radius curved one. Hence, the ideal projection can be determined by calculating the analytical function of a straight line together with the analytical function of a circle that better approximate the measured track centerline. This function is defined in Eq. 10 as follows:

$$\mathbf{r}(s)=\begin{cases}\mathbf{r}_A+\dfrac{\mathbf{r}_B-\mathbf{r}_A}{|\mathbf{r}_B-\mathbf{r}_A|}s & if \quad s\le s_1\\ \mathbf{r}_C+R\left[\cos\left(\beta+\dfrac{s-s_1}{R}\right) \quad \sin\left(\beta+\dfrac{s-s_1}{R}\right)\right]^T & if \quad s>s_1\end{cases} \tag{10}$$

In Eq. 10, $\mathbf{r}_A$ is the position vector of the initial point *A*, $\mathbf{r}_B$ is the position vector of point *B* that joins the tangent and the curved stretches, $\mathbf{r}_C$ is the position vector of the center of the curved stretch, s refers to the trajectory coordinate, s_1 is the trajectory coordinate where the curved stretch

starts, R is the curve radius and β is the orientation angle that defines the beginning of the curve as shown in Fig. 14.

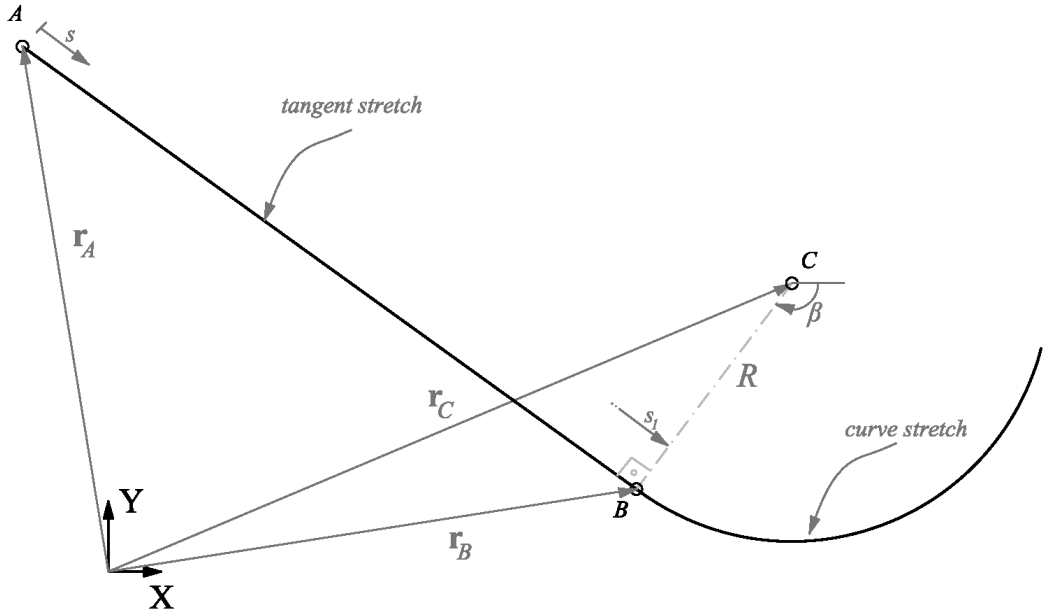

Figure 14. Ideal track centerline projection

In order to compute all parameters in Eq. 10, a minimization of the quadratic distance between the measured centerline $\mathbf{r}_{CL}$ and the ideal one $\mathbf{r}$ of Eq. 10 subject to geometrical constraints can be derived. This quadratic distance d^{i2} for each measured point i is defined similar to Eq. 5 as:

$$d^{i2} = \left[\mathbf{r}_{CL}^{i} - \mathbf{r}\left(s^{i}\right)\right]^{T}\left[\mathbf{r}_{CL}^{i} - \mathbf{r}\left(s^{i}\right)\right] \tag{11}$$

Therefore, the function f that must be minimized can be written similarly to Eq. 6 as the sum of all quadratic distances d^{i2} that depends on the unknown parameters defined Eq. 10. This is, $f = f(\mathbf{u})$, where $\mathbf{u}$ contains the unknown Cartesian components of point B and C (x_B, y_B, x_C and y_C) together with the radius of curvature R. This is, $\mathbf{u} = [x_B, y_B, x_C, y_C, R]^T$.

As this function minimization is subject to geometric constraints, the method of Lagrange multipliers [28] can be adopted where one has the following system of 7 non-linear algebraic equations.

$$\begin{gathered}\frac{\partial f(\mathbf{u})}{\partial \mathbf{u}} + \boldsymbol{\lambda}\frac{\partial \mathbf{g}(\mathbf{u})}{\partial \mathbf{u}} = \mathbf{0} \\ \mathbf{g}(\mathbf{u}) = \mathbf{0}\end{gathered} \tag{12}$$

In Eq. 12, $\boldsymbol{\lambda}$ is the vector of Lagrange multipliers associated with the vector of geometric constraints equations $\mathbf{g}$, which states that the distance between the center of the circle and the end of the tangent stretch is the radius of the circle and that the tangent vector at the beginning of the curve is normal to the position vector that joins the center of the radius with the beginning of the curve. These two constraints equations are defined as:

$$\mathbf{g}(\mathbf{u}) = \begin{cases} (x_C - x_B)^2 + (y_C - y_B)^2 - R^2 = 0 \\ (\mathbf{r}_B - \mathbf{r}_A)^T (\mathbf{r}_C - \mathbf{r}_B) = 0 \end{cases} \tag{13}$$

In this particular case, the minimization results in a total tangent stretch of s_1 = 34.85 m and a curve one of radius R = 14.92 m, which are in accordance to construction drawings.

Development:

An analytical definition of the vertical profile is achieved by straight lines with different slopes that pass through identified vertices. In these vertices, which join two consecutive lines with different slopes, there is a transition stretch obtained by a curve tangent to both lines. The procedure to obtain the transition curve between two lines, line i and line i + 1 is shown in Fig. 15 and described as:

- The transition stretch between two consecutive lines is achieved by a quadratic polynomial of the form:

$$z(s_1) = as_1^2 + bs_1 + c \tag{14}$$

where s_1 is the local trajectory parameter of Fig. 15, R_v is the vertical radius of the transition stretch, s_m and s_M are the initial and final points where the transition takes place and α^i and α^{i+1} are the angles with respect to the horizontal of lines i and i + 1 respectively. In addition, a, b and c are the polynomial coefficients.

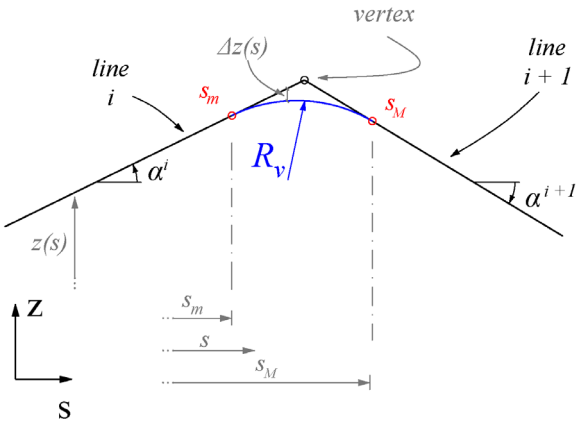

Figure 15. Vertical transition in the ideal track centerline development

- In order to fully determine the transition stretch, the four unknowns s_m, s_M, α^i and α^{i+1} have to be calculated. This is done by solving the four nonlinear equations **C** of Eq. 15.

$$\mathbf{C} = \begin{bmatrix} z^i_{line}(s_m) - z(s_m) \\ z^{i+1}_{line}(s_M) - z(s_M) \\ z'(s_m) - \alpha^i \\ z'(s_M) - \alpha^{i+1} \end{bmatrix} = \mathbf{0} \tag{15}$$

Equation 15 states that the positions of the vertical coordinates at the beginning and at the end of the transition stretch, $z(s_m)$ and $z(s_M)$, occupy the same positions as those obtained in the tangent lines. It also states that the first derivative of the transition stretch,

both at the beginning and at the end, $z'(s_m)$ and $z'(s_M)$, coincide with the slopes of the lines i and $i + 1$ respectively.

This track development procedure is applied to the scaled track after the identification of 17 different vertices. Table 3 shows the parameters needed to compute such track development.

Table 3. Parameters used in the definition of the track development

s [m]	z_{vertex} [mm]	R_v [m]	tan α^{i+1}
0,00	0,00	0,00	-0,00010873
11,06	-44,067481	600	-0,00010873
17,20	-44,7350959	-300	-0,00800532
19,94	-66,6696854	300	-0,00157755
22,20	-70,2349445	500	0,00223998
24,18	-65,7997828	100	0,01450823
26,42	-33,3013445	-50	-0,00853771
27,78	-44,9126247	50	0,0023683
31,18	-36,8604145	200	0,00800979
32,44	-26,7680822	-150	0,00052663
37,18	-24,2718432	800	0,00222553
43,24	-10,7851049	200	0,01369653
48,46	60,7107628	-100	-0,00663193
55,00	17,3379393	100	0,00068662
57,18	18,8347616	150	0,00725257
59,16	33,1948544	-100	-0,0013333
62,42	28,8482992	0,00	0,00

Super-elevation

The scale track has no cant angle definition, which implies that the ideal left and right rails has the same vertical component.

5.4 CALCULATION OF THE SCALED TRACK IRREGULARITIES

Applying the methodology detailed at Section 4, lateral and vertical irregularities are quantified. This allows to use Eq. 2 to fully define the geometry of the 5-inch gauge railroad track in terms of the well-known track characteristics of track gauge variation ζ_g, lateral alignment ζ_a, cross level ζ_{cl}, and vertical profile ζ_{vp}. These four track characteristics related to the measured scaled track are presented in Fig. 16.

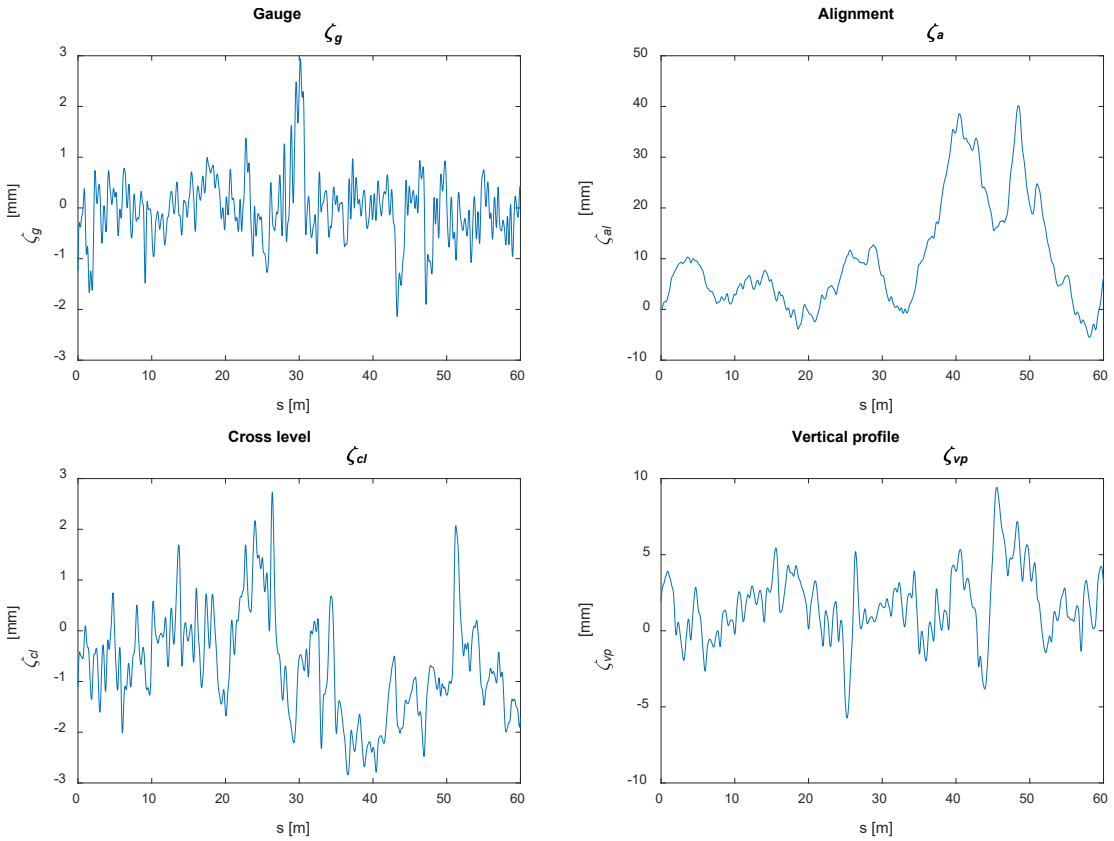

Figure 16. Scaled track irregularities features

5.5 COMPARISON WITH RESPECT TO FULL SCALE RAILROAD TRACKS

The 2-cm measurement distance between marked points involves a sampling distance frequency Ω of 50 m^{-1} that, according to Nyquist theorem allows to account for defect frequencies up to 25 m^{-1}. This is, the lowest measurable wavelength of track defects in the scaled track is up to 4 cm, which is a wider range of possible track defects with respect to measured track defects at full scale railroad tracks [2].

However, before making a comparison between the measured track defects at the scaled track with respect to full scale tracks, a simple scaling strategy can be applied. Following similarity laws [29], the decisive scaling factor that relates both real and scaled track is the length scaling factor ρ_L that linearly relates real and scaled track defects. Since the nominal gauge of the scaled track is 5 in., the length scaling factor ρ_L with respect to a standard 1435 mm gauge track is:

$$\rho_L = \frac{1435\text{mm}}{127\text{mm}} = 11.3 \tag{16}$$

which means that the amplitude and wavelength of the scaled track defects should be multiplied by ρ_L in order to be comparable with respect to full scale track defects.

Since track irregularities can be understood as a random stochastic process, one can find in the literature analytical expressions of the power spectral density functions (PSD) that describe them. As mentioned in Section 1, in [3], the measurements made by the German Railways Deutsche

Bahn AG can be seen by the PSD functions shown in Fig. 17 of the vertical profile S_{vp}, alignment S_a and cross level S_{cl} as a function of the spatial frequency Ω.

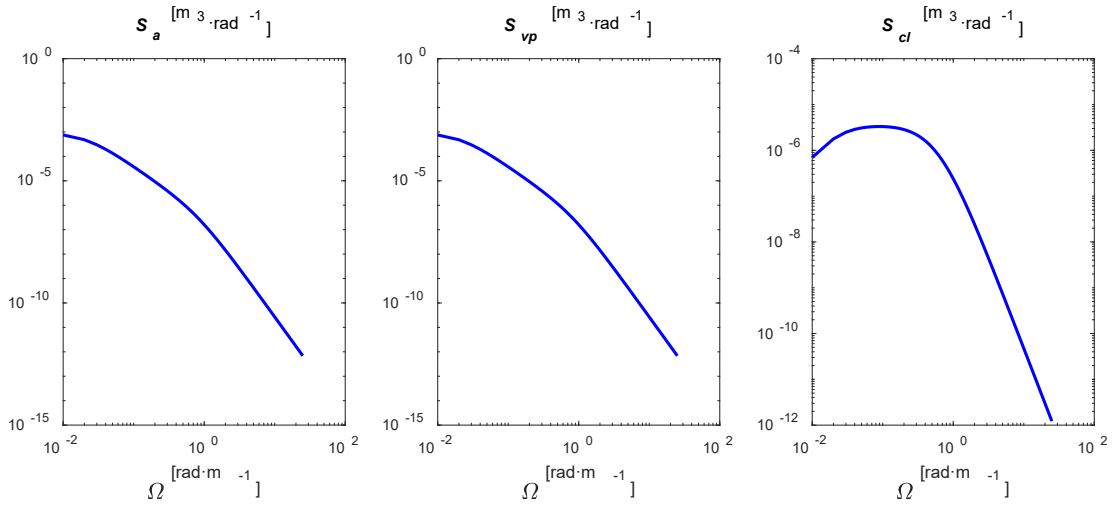

Figure 17. Analytical PSD functions of track defects at full scale railroad tracks [2]

If the measured track irregularities (amplitude and wavelength) are updated with the length scaling factor ρ_L, one can calculate the PSD functions and compare to the analytical PSD functions of Fig. 17. This comparison is made along Figs 18-20.

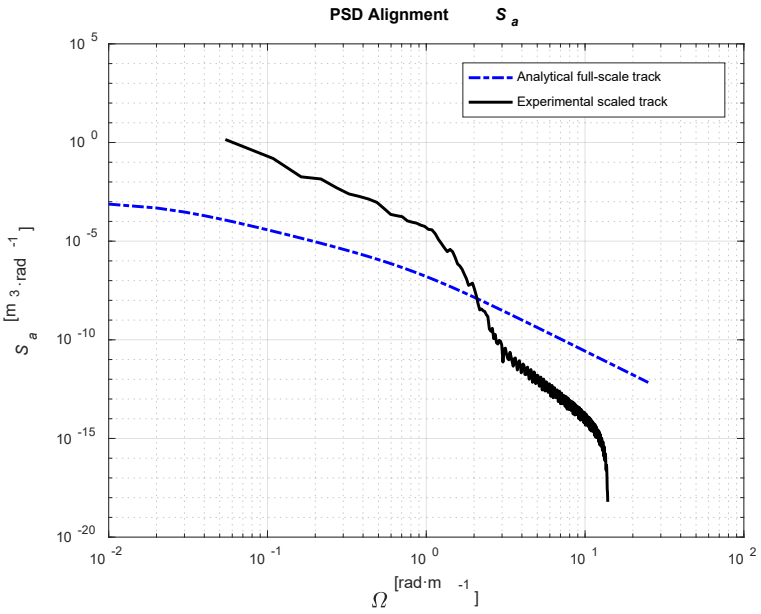

Figure 18. Alignment PSD comparison

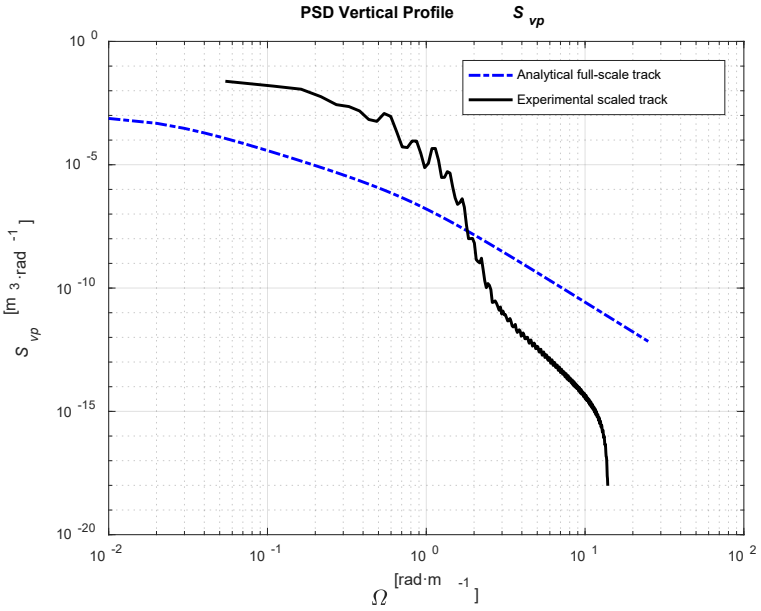

Figure 19. Vertical profile PSD comparison

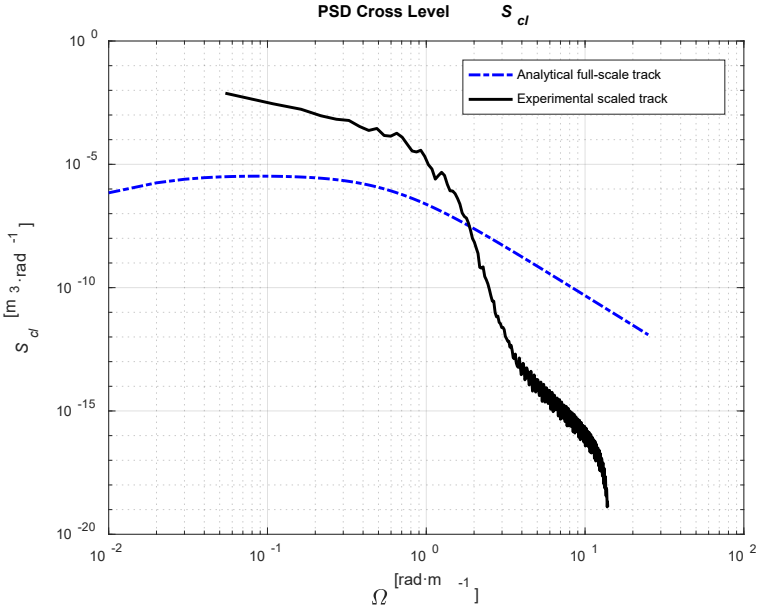

Figure 20. Cross level PSD comparison

Some conclusions can be extracted from Figs. 18-20. First, the amplitude of track defects is clearly higher in the scaled track than full scale ones (once they are updated with the scaling factor ρ_L of Eq. 16), especially if the comparison is derived in the range of $0.25 < \Omega < 2.09$ rad·m^{-1}, which is the range used for the lowest track defect wavelength *D1* according to the European Standard EN 13848 series [3]. This is explained by the fact that the scaled track was not designed for research purposes and that the accuracy in the construction was not a relevant issue. However, due to the influence that track geometry has on the dynamic behavior of railroad vehicles, the difference between the measured scaled track geometry and the estimated one [2] augments the

necessity of this measurement, especially when experimental tests to validate computational models are supposed to be done in this scaled track.

6. CONCLUSION

The results obtained in this work show that the method used to measure railroad track geometry has allowed to identify the ideal track centerline geometry and quantify defects of 4-cm minimum wavelength by using a topographic total station. The accurate results given by this method are especially required as inputs in railroad computational models, when the comparison between experimental and numerical results seeks the validation of these models. This makes the proposed method appropriate for laboratory tracks or short tracks where experimental tests take place. Based on the experimental results, the authors formulate the following conclusions and limitations:

I. It was observed that scaled or laboratory tracks used in the dynamic study of railroad vehicles can present defects higher than those predicted by PSD functions at full scale tracks.
II. The minimum defect wavelength detected by the proposed method depends on the distance between consecutive measured points on railheads. This distance can be varied to allow the determination of irregularities in different ranges of categories according to different standards [4, 5].
III. The method is limited to measure static track defects. Others such as sleeper void or fastener loosening can be determined by analyzing the dynamic behavior of vehicles running on these measured tracks.
IV. The method is also limited to short track segments due to the time needed to develop the point measurements with the topographic total station.

ACKNOWLEDGEMENTS

This work was supported by the Spanish Ministry of Science, Innovation and Universities under the project TRA2017-86355-C2-1-R. This support is gratefully acknowledged. We also thank Prof. Cristina Torrecillas for her valuable contribution to the experimental measurement. Finally, authors would like to express their gratitude to the group “Asociación Sevillana de Amigos del Ferrocarril” (*www.asaf.es/indexalamillo.html*), who kindly provided the access and use of their facilities.

REFERENCES

[1] Zhai, W., Wang, K., & Cai, C. (2009). Fundamentals of vehicle–track coupled dynamics. *Vehicle System Dynamics*, *47*(11), 1349-1376.
[2] Frýba, L. (1996). *Dynamics of railway bridges*. Thomas Telford Publishing.
[3] Claus, H., & Schiehlen, W. (1998). Modeling and simulation of railway bogie structural vibrations. *Vehicle System Dynamics, 29*(S1), 538-552.
[4] CEN – CENELEC Management Centre. European Standard EN 13848 series. (2009) Railway applications – Track – Track geometry quality. Parts 1 – 6.

[5] FRA, Federal Railway Administration (2013). Vehicle/Track Interaction Safety Standards; High-Speed and High Cant Deficiency Operations. U.S. Department of Transportation, Office of Safety Research, Washington, D.C.

[6] Garg, V. K., & Dukkipati, R. V. (1984). Dynamics of railway vehicle systems. Academic press.

[7] Fries, R. H., & Coffey, B. M. (1990). A state-space approach to the synthesis of random vertical and crosslevel rail irregularities. *Journal of dynamic systems, measurement, and control, 112(1),* 83-87.

[8] Perrin, G., Soize, C., Duhamel, D., & Funfschilling, C. (2013). Track irregularities stochastic modeling. *Probabilistic Engineering Mechanics*, *34*, 123-130.

[9] Iyengar, R. N., & Jaiswal, O. R. (1993). A new model for non-Gaussian random excitations. *Probabilistic engineering mechanics*, *8*(3-4), 281-287.

[10] Stow, J. & Andersson, E. (2006). Field Testing and Instrumentation of Railway Vehicles. In: S. Iwnicki (editor), *Handbook of Railway Vehicle Dynamics*, 424-456. CRC Press.

[11] Yao, L., Zhou, Y., Li, N., & Sun, P. (2015). Detection of high speed railway track static regularity with laser trackers. Survey *Review, 47:343,* 279-285. DOI: 10.1179/1752270614Y.0000000135

[12] Psimoulis, P. A., & Stiros, S. C. (2013). Measuring deflections of a short-span railway bridge using a robotic total station. *Journal of Bridge Engineering, 18(2),* 182-185.

[13] Psimoulis, P. A., & Stiros, S. C. (2007). Measurement of deflections and of oscillation frequencies of engineering structures using Robotic Theodolites (RTS). *Engineering Structures, 29(12),* 3312-3324.

[14] Chen, Q., Niu, X., Zuo, L., Zhang, T., Xiao, F., Liu, Y., & Liu, J. (2018). A railway track geometry measuring trolley system based on aided INS. *Sensors*, 18(2), 538.

[15] Akpinar, B., & Gulal, E. (2012). Multisensor railway track geometry surveying system. *IEEE Transactions on Instrumentation and Measurement*, 61(1), 190-197.

[16] Akpınar, B., & Gülal, E. (2013). Railway track geometry determination using adaptive Kalman filtering model. *Measurement, 46*(1), 639-645.

[17] Weston, P., Roberts, C., Yeo, G., & Stewart, E. (2015). Perspectives on railway track geometry condition monitoring from in-service railway vehicles. *Vehicle System Dynamics*, *53*(7), 1063-1091.

[18] Westeon, P. F., Ling, C. S., Roberts, C., Goodman, C. J., Li, P., & Goodall, R. M. (2007). Monitoring vertical track irregularity from in-service railway vehicles. *Proceedings of the institution of mechanical engineers, Part F: Journal of Rail and Rapid Transit*, *221*(1), 75-88.

[19] Weston, P. F., Ling, C. S., Goodman, C. J., Roberts, C., Li, P., & Goodall, R. M. (2007). Monitoring lateral track irregularity from in-service railway vehicles. *Proceedings of the Institution of Mechanical Engineers, Part F: Journal of Rail and Rapid Transit*, *221*(1), 89-100.

[20] Tsunashima, H., Naganuma, Y., Matsumoto, A., Mizuma, T., & Mori, H. (2012). Condition monitoring of railway track using in-service vehicle. In *Reliability and safety in railway*. InTech.

[21] Karis, T., Berg, M., Stichel, S., Li, M., Thomas, D., & Dirks, B. (2018). Correlation of track irregularities and vehicle responses based on measured data. *Vehicle System Dynamics*, *56*(6), 967-981.

[22] Taheri Andani, M., Peterson, A., Munoz, J., & Ahmadian, M. (2018). Railway track irregularity and curvature estimation using doppler LIDAR fiber optics. *Proceedings of the*

Institution of Mechanical Engineers, Part F: Journal of Rail and Rapid Transit, *232*(1), 63-72.

[23] Nielsen, J., Berggren, E., Lölgen, T., Müller, R., Stallaert, B., & Pesqueux, L. (2013). Overview of methods for measurement of track irregularities important for ground-borne vibration. *RIVAS Deliverable*, *2*.

[24] Norén-Cosgriff, K., Berggren, E. G., Kaynia, A. M., Dam, N. N., & Mortensen, N. (2018). A new method for estimation of critical speed for railway tracks on soft ground. *International Journal of Rail Transportation*, 1-15.

[25] Zhu, S., & Cai, C. (2014). Interface damage and its effect on vibrations of slab track under temperature and vehicle dynamic loads. *International Journal of Non-Linear Mechanics*, *58*, 222-232.

[26] Rathod, C., & Shabana, A. A. (2007). Geometry and differentiability requirements in multibody railroad vehicle dynamic formulations. Nonlinear Dynamics, 47(1-3), 249-261.

[27] Chen, Q., Niu, X., Zhang, Q., & Cheng, Y. (2015). Railway track irregularity measuring by GNSS/INS integration. *Navigation: Journal of The Institute of Navigation*, *62*(1), 83-93.

[28] Bertsekas, D. P. (2014). Constrained optimization and Lagrange multiplier methods. Academic press.

[29] Bosso, N., Gugliotta, A., & Soma, A. (2002). Comparison of different scaling techniques for the dynamics of a bogie on roller rig. *Vehicle System Dynamics*, *37*(sup1), 514-530.